Article

Discrete Element Simulation Analysis of Biaxial Mechanical Properties of Concrete with Large-Size Recycled Aggregate

Tan Li [ID] **and Jianzhuang Xiao** *

Department of Structural Engineering, Tongji University, Shanghai 200092, China; litan@tongji.edu.cn
* Correspondence: jzx@tonji.edu.cn

Abstract: Concrete made with large-size recycled aggregates is a new kind of recycled concrete, where the size of the recycled aggregate used is 25–80 mm, which is generally three times that of conventional aggregate. Thus, its composition and mechanical properties are different from that of conventional recycled concrete and can be applied in large-volume structures. In this study, recycled aggregate generated in two stages with randomly distributed gravels and mortar was used to replace the conventional recycled aggregate model, to observe the internal stress state and cracking of the large-size recycled aggregate. This paper also investigated the mechanical properties, such as the compressive strength, crack morphology, and stress–strain curve, of concrete with large-size recycled aggregates under different confining pressures and recycled aggregate incorporation ratios. Through this research, it was found that when compared with conventional concrete, under the confining pressure, the strength of large-size recycled aggregate concrete did not decrease significantly at the same stress state, moreover, the stiffness was increased. Confining pressure has a significant influence on the strength of large-size recycled aggregate cocrete.

Keywords: concrete with large-size recycled aggregate; biaxial mechanical properties; discrete element method; PFC

1. Introduction

Not only does waste concrete take up much space, but it also pollutes the environment. This trend has accelerated dramatically as the economy has grown. As a result, how to recycle unwanted concrete has become a global issue with significant social, economic, and environmental implications. Utilizing waste concrete as recycled aggregate for the production of recycled concrete is currently the most sustainable alternative. Scholars have studied the mechanical qualities and durability of recycled coarse concrete for decades [1–4] and explained that the recycled concrete's mechanical properties deteriorate from the aspects of the microstructure and the failure mechanism [5,6]. The research on recycled concrete has now been broadened to include high-performance concrete [7,8]. However, because recycled aggregate production requires numerous crushing and screening procedures, the cost of production is relatively expensive. Increasing the size of recycled aggregate (RA) can reduce the cost of producing recycled concrete and enhance resource use efficiency. As a result, Li et al. [9] showed that crushing discarded concrete into bigger particle size recycled coarse aggregate (RCA) and mixing it with recycled concrete does not lead to a degradation of the recycled concrete's fundamental mechanical properties. Steel bars with suitable spacing are used in big-volume concrete projects, and concrete projects with a low reinforcement ratio have a high application value. In addition to dams in water conservancy projects, breakwaters and wharves in port projects, and piers and shields in traffic projects, shielding structures in nuclear engineering and bunkers in military engineering all have vast applications. Certain large-volume concrete members exhibit a variety of stress states. To advance their applications, it is vital to investigate the mechanical characteristics of these materials under multiaxial stress states.

At the moment, there are numerous methods for simulating recycled concrete. The discrete element method is one of the techniques that has been examined in the research of recycled concrete damage. The discrete element method considers the materials to be a discrete, discontinuous medium. The elements in the discrete element technique have normal and tangential stiffness, which are used to model the interaction between the elements, and the normal and tangential bonding strengths between the elements can be adjusted to simulate the elements cracking. Recent versions of the discrete element technique employ deformable blocks to overcome high joint displacements and modest block deformations [10–13]. He et al. [14] conducted biaxial compression experiments on recycled concrete at various strain rates and discovered that while the strength of RAC rose as the strain rate increased, the concrete's failure mode remained the same. Ying et al. [15] employed the three-dimensional base force element technique (BFEM) to simulate the uniaxial compression test of recycled concrete, and the results demonstrated that the method could accurately represent the nonlinear deformation of RAC. Yu et al. [16] analyzed the compression failure of recycled concrete using the discrete element approach. The material qualities of aggregate, recycled aggregate, mortar, aggregate damage, and ancient mortar content were examined. According to studies, the relative strength of the old and new mortars is critical in refining the RAC's failure mechanism. Peng et al. [17] compared the five-phase spherical model's mechanical properties to those of the random aggregate model. Both are in good accord with one another and with current experimental evidence. Tan et al. [18] studied the cracking process of model recycled concrete using the discrete element method and found that compared to the cracking model measured in the experiment, the shear strength of the interfacial transition zone (ITZ) has the most significant strength influence on the macromechanical behavior. Li et al. [19] examined the finite element approach with the discrete element method for simulating large-size recycled aggregate concrete and found that the discrete element method produces more realistic results at a larger recycled aggregate inclusion ratio. This technique has been frequently applied to the stress cracking of rock materials, with excellent results.

These investigations are still limited to recycled aggregates with a simple internal composition, or the models employed do not adequately describe the impact of internal structure in recycled aggregates on concrete mechanical properties. Because the maximum size of recycled aggregate used in concrete made with large-size recycled concrete is 80 mm, which is more than three times the size of the conventional aggregate used in the original concrete, more sophisticated models are required to accurately explain the composition of recycled aggregates. Because of the vast range of uses for this type of concrete, many of them are complex in nature with larger specimen, which is larger than most multiaxis mechanical testing equipment' size requirements. As a result, recycled aggregate generated in two stages with randomly dispersed gravels and mortar was utilized to replace the standard recycled aggregate model in this paper, and it was used to simulate the specimen under biaxial force. This article also looked at the compressive strength, crack morphology, and stress–strain curve of concrete using large-size recycled aggregate under various confining pressures and recycled aggregate incorporation percentages.

2. Model Building

2.1. Generating the Random Aggregate Model

In this article, the size of the specimen and the internal composition of the recycled concrete reflect the size effect of concrete with large-size recycled aggregate. The specimen size used in this article was 300 mm × 300 mm × 300 mm, which is larger than the conventional specimen size of 150 mm × 150 mm × 150 mm. In addition, the difference in aggregate size is also reflected in the recycled aggregate. The model of the large-size recycled aggregate is different from the conventional recycled aggregate model that is mainly gravel-adhered old mortars, the large-size recycled aggregate model contains more conventional sized gravels. The cracked section of the specimen (300 mm × 300 mm × 300 mm) of concrete with large size recycled concrete aggregates in the test is depicted in

Figure 1. The greatest aggregate size that can be used is 80 mm. To distinguish recycled aggregate, the surface was colored with red ink. It is a darker shade than the nearby cement paste. As can be observed, recycled aggregate has a more complicated structure and resembles concrete blocks in composition. The visual characteristics of the large-size recycled aggregate are depicted in Figure 2. In the illustration, RCA denotes recycled coarse aggregate, OM denotes old mortar, and NM denotes new mortar. Old ITZ denotes the interface transition zone (ITZ) between natural aggregate and old mortar within the recycled aggregate, while New ITZ denotes the interface transition zone (ITZ) between recycled aggregate and new mortar. As can be seen, the large-size recycled aggregate is complicated in structure; uneven in appearance; porous, angular, and rough on the surface; and contains several gravels. The visual features of regenerated aggregates of conventional size are depicted in Figure 3. Compared to typically recycled aggregate, its surface is rough and porous, but it lacks sharp edges and corners due to its bigger size.

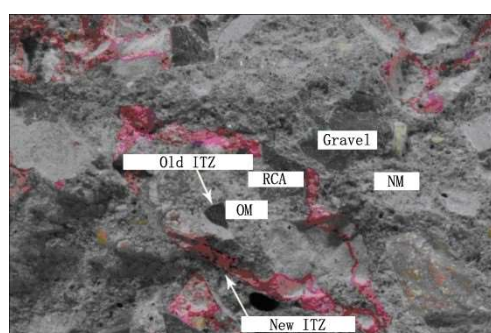**Figure 1.** The internal structure of large-size RA recycled concrete.

Figure 2. The shape of large-size RA.

Figure 3. The shape of conventional-size RA.

The Monte Carlo method was adopted in the model for the position and size of aggregates. The Walraven formula was adopted to grade natural coarse aggregates in the concrete random aggregate model. The general expression of the formula is as follows [20]:

$$p_c(D < D_0) = p_k(1.065D_0^{0.5}D_{\max}^{-0.5} - 0.053D_0^4 D_{\max}^{-4} - 0.012D_0^6 D_{\max}^{-6} - 0.0045D_0^8 D_{\max}^{-8} - 0.0025D_0^{10}D_{\max}^{-10}) \quad (1)$$

Take ξ to be a random number in the interval [0, 1]. If $\xi = p_c$ is used, it is difficult to solve D_0. Therefore, a gradation curve is drawn in the gradation interval of 5~25 mm and then a polynomial is used to fit the method, and the curve is shown in Figure 4. The inverse function of the curve is

$$D = 0.1074p_c^6 - 0.2749p_c^5 + 0.274p_c^4 - 0.1254p_c^3 + 0.0315p_c^2 + 0.0138p_c + 0.0048 \quad (2)$$

Let $\xi = p_c$, then we get

$$D = 0.1074\xi^6 - 0.2749\xi^5 + 0.274\xi^4 - 0.1254\xi^3 + 0.0315\xi^2 + 0.0138\xi + 0.0048 \quad (3)$$

Through the formula obtained by the above fitting, the content of the natural coarse aggregate of each size is calculated, and the aggregates meeting the gradation requirements are generated by the previous method to prepare for the subsequent aggregate placement. The gradation of recycled aggregate is determined by a similar method.
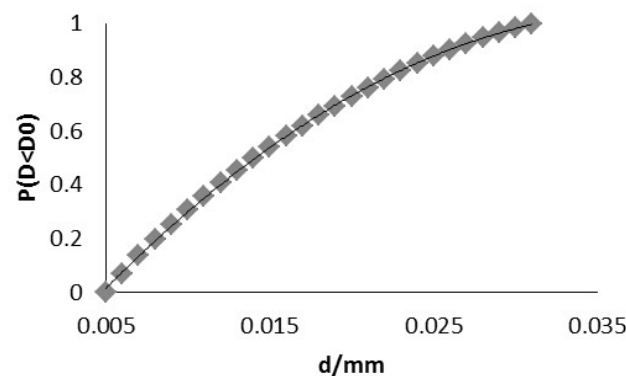

Figure 4. Gradation fitting curve in the interval of 5~31.5 mm.

The aggregate generation method determines the amount of natural coarse aggregate and recycled aggregate necessary for each size using the Wallachian formula, organizes them in size order, and places them in the target area using the Monte Carlo approach. Each time an aggregate is placed, its overlap with the current aggregate in the target region is determined. If there is overlap, the placement of aggregate is adjusted and is re-inserted. The aggregate generating process goes on until all aggregates are placed in the target area.

Due to the huge size of the recycled aggregate, which contains numerous gravels, the simulation takes the gravel distribution inside the recycled aggregate into account. Because a portion of the recycled aggregate is fractured during the test, it is vital to analyze gravel and old mortar distribution in the recycled aggregate. To accurately portray the distribution of gravels in the recycled aggregate, the created model is formed of gravels and mortars of varying sizes and amounts.

This article employs a two-stage random aggregate generation and distribution method, which entails randomly producing aggregates in the recycled concrete model twice and then deleting them to acquire the recycled aggregate's fine structure and construct the recycled concrete model. The entire process of creating a recycled concrete model consists of three parts, as illustrated in Figure 5, namely generate RA and NA, regenerate NA, and eliminate noncompliant NA. The following are the detailed steps:

Step 1: Determine the quantity and size of recycled aggregates according to the incorporation ratio and gradation of recycled coarse aggregate (RCA), and generate recycled aggregates one by one and place them in the model space, the rest of the gravels are calculated according to the grading formula, and from large to small placed in the model space.

Generate RA and NA

Step 2: Generate aggregates according to the aggregate grade of recycled coarse aggregate, and place them in the model space from large to small.

Generate NA again

Step 3: Delete the second-placed aggregate that is outside of the recycled aggregate.

Delete non-compliant NA

Figure 5. Process of building the recycled concrete model.

The random aggregate model was finally generated through the above two steps, and some examples are shown in Figure 6. The black area in the figure is mortar, the gray area is recycled aggregate, and the white area is natural coarse aggregate. Since recycled aggregate and new concrete use the same kind of stones, no distinction was made in the model.

(**a**) 0 RA

(**b**) 10% RA

(**c**) 20% RA

(**d**) 30% RA

(**e**) 40% RA

Figure 6. The geometric model of different recycled coarse aggregates.

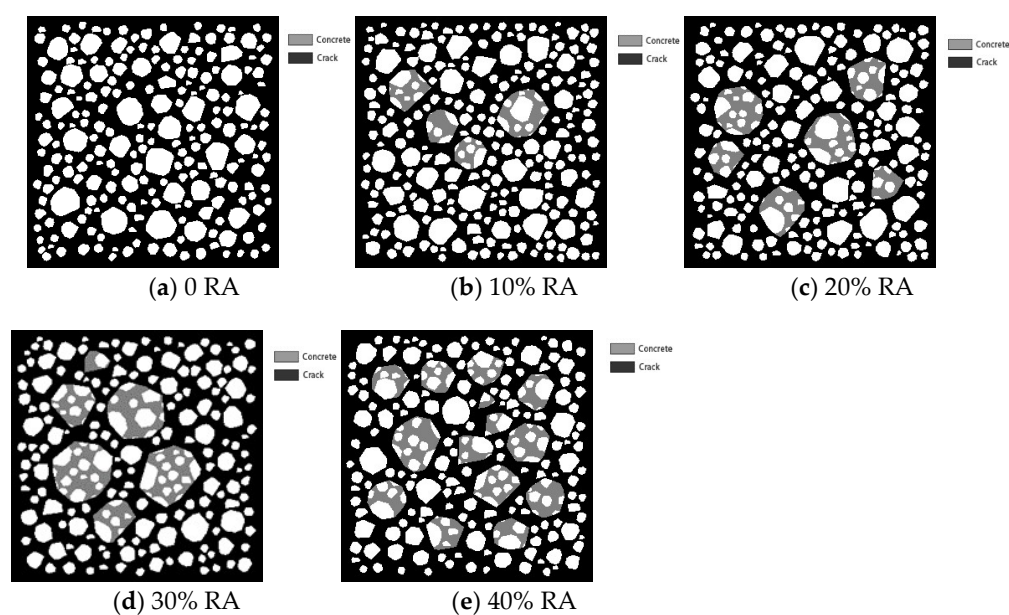### 2.2. Building a Discrete Element Model

The simulation used the commercial discrete element calculation software, PFC. Using the method shown in Figure 5, discrete element models made of elements from six different materials types were created using the incorporation ratios of 0, 10%, 20%, 30%, and 40% of recycled aggregate. The various material types used in this investigation were gravel, old mortar, new mortar, the ITZ between gravel and old mortar, the ITZ between gravel and new mortar, and the ITZ between new and old mortar. The models are illustrated in Figure 7, in which the black area represents new mortar, the white area represents natural coarse aggregate, and the gray area represents recycled aggregate mortar. Material parameter values are listed in Table 1.
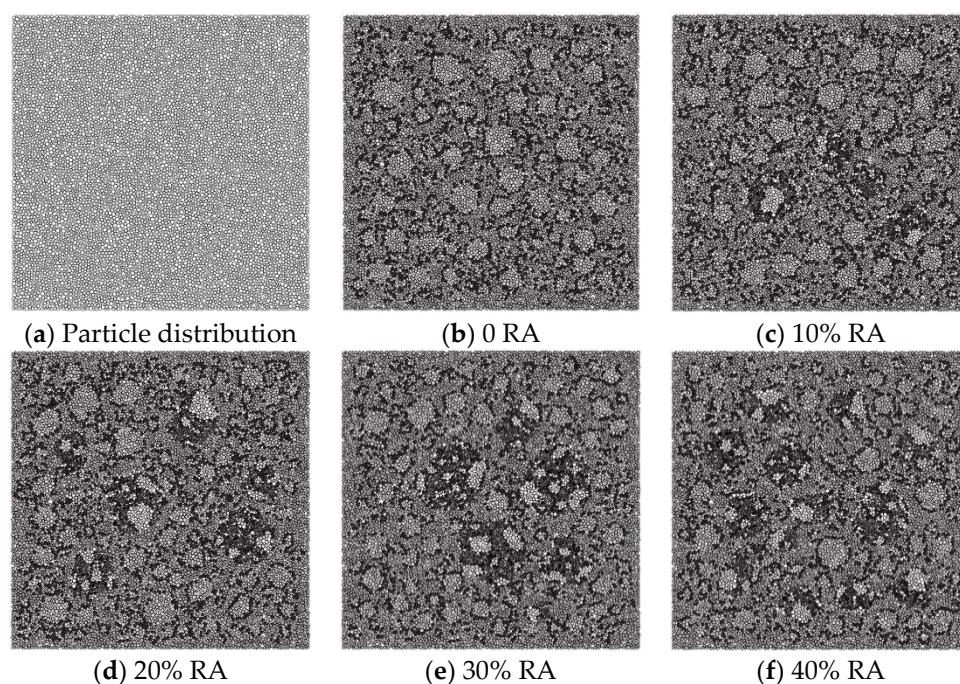

| (**a**) Particle distribution | (**b**) 0 RA | (**c**) 10% RA |
| (**d**) 20% RA | (**e**) 30% RA | (**f**) 40% RA |

Figure 7. Discrete element model of recycled concrete.

To identify the test specimens (or simulation models) used to determine the strength of concrete, the following labeling sequence was used: The label begins with the letter C, which denotes how recycled concrete is prepared. The final six digits represent the strength grade of the existing concrete (two digits), the mixing ratio of the existing concrete (two digits), and the strength grade of the new concrete (two digits). Furthermore, the following method was adopted to number the simulation models used to determine the stress–strain relationship of concrete under lateral pressure: The model number begins with P and represents the confining pressure (MPa), followed by C, which contains information about how recycled concrete is prepared. The final six digits represent the strength of the existing concrete (two digits), the mixing ratio of the existing concrete (two digits), and the strength grade of the new concrete (two digits).

A test model of random particle distribution was built using the height of the specimen, the maximum and minimum radius, the stiffness ratio, and other information. The model's porosity was fixed to 16% to ensure its tightness. The model was constructed by randomly distributing particles inside the model region that meet the particle size requirements. The produced particles were approximately one millimeter in diameter. The expansion approach was used in the granular delivery method. First, the required number of particles was determined based on the particle distribution and the specimen area (300 mm × 300 mm). Then the radius of these particles was lowered to 0.625 times their original size and they were dropped equally into the specimen area, being careful not to overlap the particles. Following delivery, the size of all particles was multiplied by 1.6

to restore them to their original size. Finally, a total of approximately 10,000 particles was obtained. To achieve stress balance for the particles in the model, the friction coefficient was set to zero, a confining pressure was applied, and the left and right restriction walls were modified to bring each section of the particle system to a condition of essentially equal stress in all directions. Then, using a uniform stress of less than 1% of the uniaxial compressive strength, the model's top and bottom and left and right loading walls were changed so that each point's stress state approached the given stress value, achieving an anisotropic stress state. This step aimed to eliminate the stress self-locking phenomenon in the system during the future bond generation and model unloading processes, as self-locking stress is proportional to the pressure between the particles during the bond generation process. Following that, the suspended particulate matter needed to be removed. When the model is constructed, a significant number of suspended particles will be generated, and their contact pairings with neighboring particles will be less than three. Then there is bonding formation, which encompasses both physical and parallel bonding. Physical bonds were placed between touching particles, and particles that meet the bond radius were held by parallel bonds. To minimize the impact at the moment of load application, a cycle was established for the load from the static state to the specified loading rate to increase until the specified loading rate gradually. Loading should be halted when the difference between the measured vertical and horizontal stresses and the expected stresses is less than a multiple set difference. To avoid the specimen being struck by the load abruptly, the load was separated into ten stages and loaded incrementally until it reached the predetermined pace. Figure 7a illustrates the resultant particle distribution. As observed in the image, the particle gradation is rather good, and the dispersion is fairly consistent. Assign material properties to the geometric model in Figure 6 according to the region to which the particle belongs. Figure 7b–f illustrates the final models.

2.3. Discrete Element Parameter Determination

Due to many factors in the discrete element model and the nonlinear relationship between the macroscopic mechanical properties of the materials, numerous calculations are necessary. Thus, representative test points were chosen for trial calculation, and the outcomes of the trial calculation were used to determine the following parameter selection. Finally, the optimal parameter values were derived using this procedure. To begin, an orthogonal table was built to denote the representative feature points that were to be determined. The basic mesomechanical parameters were determined from numerous articles [21]. Following completion of the calculation, the orthogonal experiment's findings were reviewed, and it was necessary that the variation range of the macromechanical parameters obtained during the calculation should include the value of the simulated material. If this condition was not satisfied, the discrete element model's parameter values needed to be changed. The adjustment approach employed multivariate statistics to determine the discrete element parameter value that had the largest effect on the macroscopic material qualities that did not match the requirements. Then, depending on whether the relationship was positive or negative, the correlation between each macro parameter and the discrete element parameter was calculated. The discrete element parameter was extended by two times or reduced to half of its original value. Then the new orthogonal table was calculated and the preceding judgment was again applied to the calculated results until the obtained macromechanical parameters met the requirements.

A neural network system with three micromechanical parameters was constructed utilizing 81 data points from the orthogonal table as training samples. Then, using the fitness function of the created neural network system, the genetic algorithm was employed to calculate the discrete element parameter values for the macromechanical parameters. Table 1 contains the final values for the discrete element parameters. Among them, Old ITZ 1 was C30 mortar and Gravel ITZ, Old ITZ 2 was C40 mortar and Gravel ITZ, New ITZ 1 was the new mortar and old mortar was C30 ITZ, New ITZ 2 was the new mortar

and old mortar was C40 ITZ, and New ITZ 3 was ITZ with C30 or C40 for the old mortar and new mortar, respectively.

Table 1. Discrete element parameters of recycled concrete.

	Gravel	C30 Mortar	C40 Mortar	Old ITZ 1	Old ITZ 2	New ITZ 1	New ITZ 2	New ITZ 3
$\overline{E}_c/\mathrm{Pa}$	55.15	27.76	35.11	22.83	29.31	22.82	27.76	23.46
$k_\mathrm{n}/k_\mathrm{s}$	2.69	2.34	2.53	2.26	2.38	2.21	2.34	2.29
$\overline{\mu}$	0.43	0.17	0.20	0.18	0.18	0.17	0.17	0.19
$\overline{\lambda}$	0.23	0.24	0.23	0.23	0.24	0.24	0.24	0.23
$\overline{E}_\mathrm{c}/\mathrm{Pa}$	135.27	47.09	67.55	40.25	54.79	43.23	47.09	43.69
$\overline{k}_n/\overline{k}_s$	0.51	0.58	0.60	0.53	0.57	0.54	0.58	0.52
$\overline{\sigma}_\mathrm{c}(\mathrm{mean})/\mathrm{Pa}$	338.12	246.10	348.15	199.43	267.51	174.69	246.10	213.84
$\overline{\sigma}_\mathrm{c}(\mathrm{std\,.dev})$	41.52	73.05	68.09	72.28	70.90	73.37	73.05	70.81
$\overline{\tau}_c(\mathrm{mean})/\mathrm{Pa}$	240.88	104.43	132.60	101.32	113.97	95.05	104.43	107.74
$\overline{\tau}_c(std.dev)$ $\overline{\tau}_\mathrm{c}(\mathrm{std\,.dev})$	51.90	49.38	42.65	53.71	48.47	55.52	49.38	53.07

3. Model Validation

The specimen measured 300 mm $\times$ 300 mm $\times$ 300 mm. The recycled aggregates were incorporated at a rate of 0, 20%, 30%, and 40%, respectively. PO 42.5 cement was utilized in the test, medium sand was employed as the sand, and basalt gravel was used as the natural coarse aggregate. A retardant and superplasticizer were used in the water to facilitate pumping. The large-size recycled aggregate was 80 mm in size and was produced by crushing leftover concrete slabs. Two size ranges were used: 25–40 and 40–80 mm. The mass ratio of the size range was fixed to 50:50 [9] using the Ping–Funk equation [22–26]. The concrete mixing ratio is provided in Table 2. The compression test was conducted following the technique for testing concrete structures (GB/T 50152-2012) [27].

Table 2. A mix ratio of concrete with LRCA.

Grade	Incorporation %	Cement kg	Water kg	Sand kg	NCA kg	LRCA kg	Superplasticizer kg
	0	286	175	924	1068	0	3.70
C30	20	270	165	871	636	480	3.49
	30	261	160	844	420	720	3.38
	40	253	155	818	204	960	3.28
	0	360	170	893	1057	0	7.00
C40	20	339	160	842	625	480	6.60
	30	329	155	817	409	720	6.40
	40	319	151	791	193	960	6.20

Table 3 compares the uniaxial compression strength of the test data to the simulation results. Figure 8 depicts the specimen following failure. As seen in the table, the simulation findings were pretty similar to the test results. The majority of data mistakes were within 10%, while some were within 5%. The value of the data error with the smallest error was smaller than 1%. It demonstrates that the constructed model is realistic, can be utilized to study recycled concrete's mechanical properties, and accurately reflects the physical and mechanical features of actually recycled concrete.

Table 3. Comparison of test value and simulation value (MPa).

Label	C300030	C302030	C303030	C304030	C400040	C402040	C403040	C404040
Test	25.76	26.43	26.87	24.47	33.25	34.83	33.37	28.51
Simulation	29.78	25.15	25.57	24.37	37.02	29.84	31.02	30.17

Figure 8. Destroyed specimen.

4. Results and Analysis

4.1. Influence of Different Incorporation Ratios under 10 MPa Confining Pressure

The compressive strength of recycled concrete in the cube under a confining pressure of 10 MPa is depicted in Figure 9. The sample number P10C denotes a lateral pressure of 10 MPa, the first two digits after C denote the strength grade of recycled aggregate in the original concrete, the middle two digits denote the recycled coarse aggregate mixing ratio, and the final two digits denote the strength grade of new concrete. Because each curve in Figure 8 contains different incorporation ratios, the legend has been changed with xx. As seen in the picture, the strength reduction of recycled concrete is not immediately apparent when lateral pressure is applied. The specimen with the most significant reduction was P10C401040, which was 15% less than that for P10C400040. The specimen with the least loss in strength was the P10C401030 specimen, which was 0.6 times weaker than the P10C400030 specimen. For instance, if both the old recycled aggregate and the new concrete are strong, adding large-size recycled aggregate results in a higher drop in strength. This could be because the ITZ in recycled aggregate is more frail and prone to cracking. When the original concrete is stronger than the new concrete, the strength loss near the ITZ is minimal, and the recycled aggregate is less prone to break.
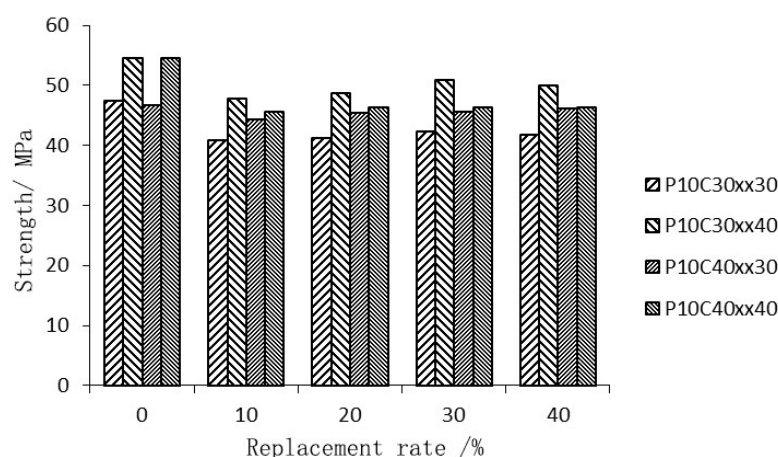

Figure 9. Compressive strength distribution at 10 MPa confining pressure.

Figure 10 illustrates the discrete model cracking at a confining pressure of 10 MPa. As observed in the illustration, the cracks in conventional concrete were square and had an angle of about 45 degrees with the horizontal direction, indicating that the concrete failed via shear cut destruction. As the amount of recycled aggregates increased, the model's crack count climbed. The cracks in the model eventually changed shape from a square to a diagonal crack that penetrated two of the model's opposing corners. This demonstrates that when the recycled coarse aggregate incorporation ratio is large, the failure mechanism of recycled concrete is similar to that of uniaxial compression. On P10C401040, the cracking

form changed more dramatically when recycled aggregate was added. This resulted in a reasonably considerable reduction in the stress exhibited in Figure 8 after the addition of recycled material. P10C301040 and P10C401030, on the other hand, had comparatively modest diagonal cracks. As seen by the tension in Figure 8, the strength difference between concrete without recycled aggregate and concrete with recycled aggregate is negligible.
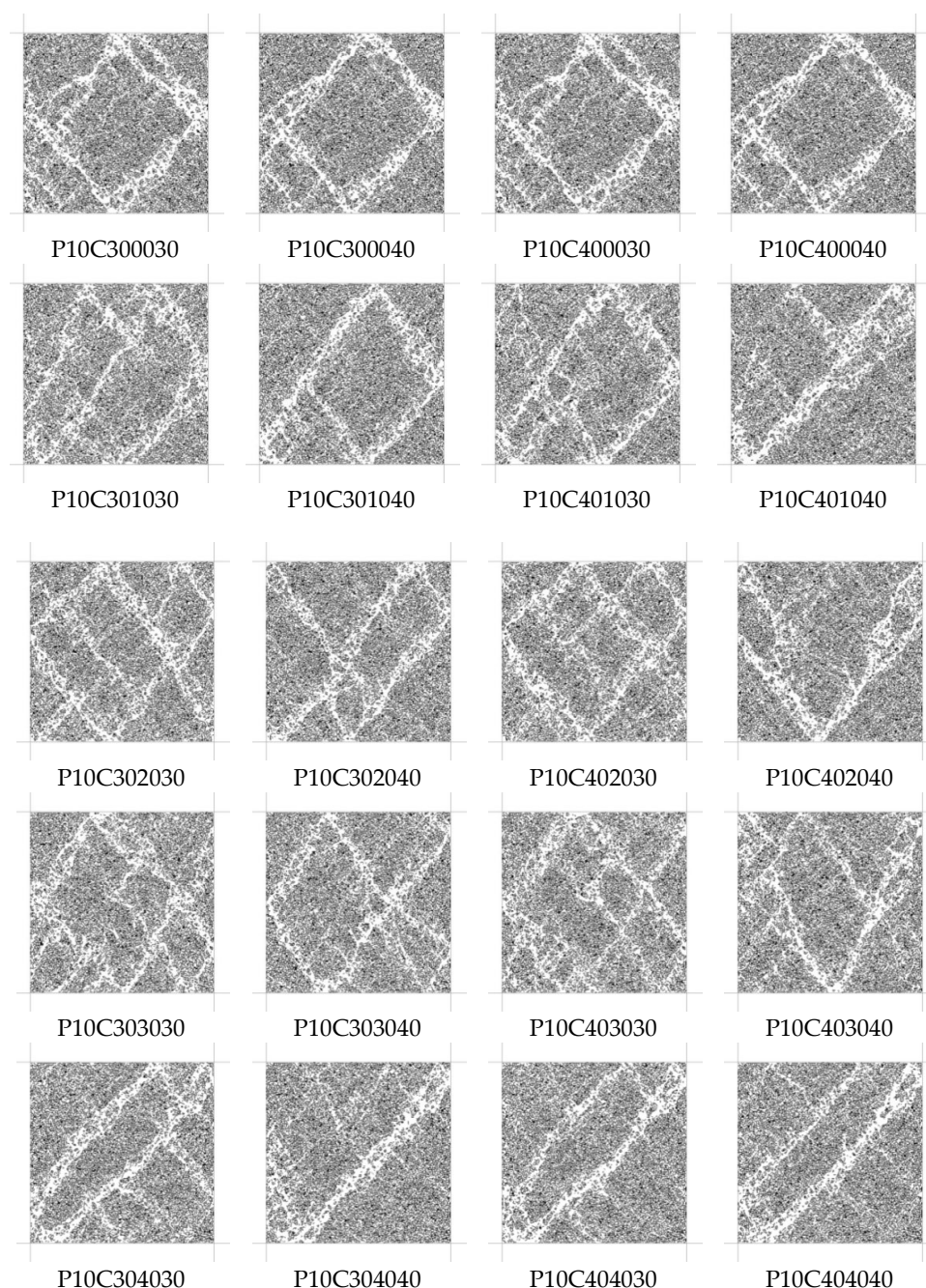

| P10C300030 | P10C300040 | P10C400030 | P10C400040 |

| P10C301030 | P10C301040 | P10C401030 | P10C401040 |

| P10C302030 | P10C302040 | P10C402030 | P10C402040 |

| P10C303030 | P10C303040 | P10C403030 | P10C403040 |

| P10C304030 | P10C304040 | P10C404030 | P10C404040 |

Figure 10. Cracking under 10 MPa confining pressure.

4.2. Stress–Strain Curve under 10 MPa Confining Pressure

Since the discrete element method cannot calculate the stress and strain in a continuum, macroscopic mechanical properties such as deformation and stress were estimated by specifying some measurement areas in the model. The stress–strain curve of concrete at a confining pressure of 10 MPa is shown in Figure 11. As shown in the picture, the stress–strain curves of conventional concrete and recycled concrete were similar when the

confining pressure was increased, and recycled concrete has a somewhat lower stress–strain curve than that of conventional concrete. It demonstrates that confining pressure has a substantial effect on recycled concrete's strength. By comparing Figure 11a,b, it is clear that the addition of large-size recycled aggregates had a higher effect on the rising region of the stress–strain curve but had a smaller effect on the falling section. When the age of the concrete was greater than the age of the new concrete, adding large-size recycled aggregate did not affect the stress–strain curve. When the old and new concrete strengths were equal, the stress–strain curve's rising portion had a higher reduction. The reason for this is because, after cracks form, recycled concrete has a higher Poisson's ratio. By increasing the confining pressure, the Poisson's ratio of recycled concrete can be reduced, hence enhancing its strength.
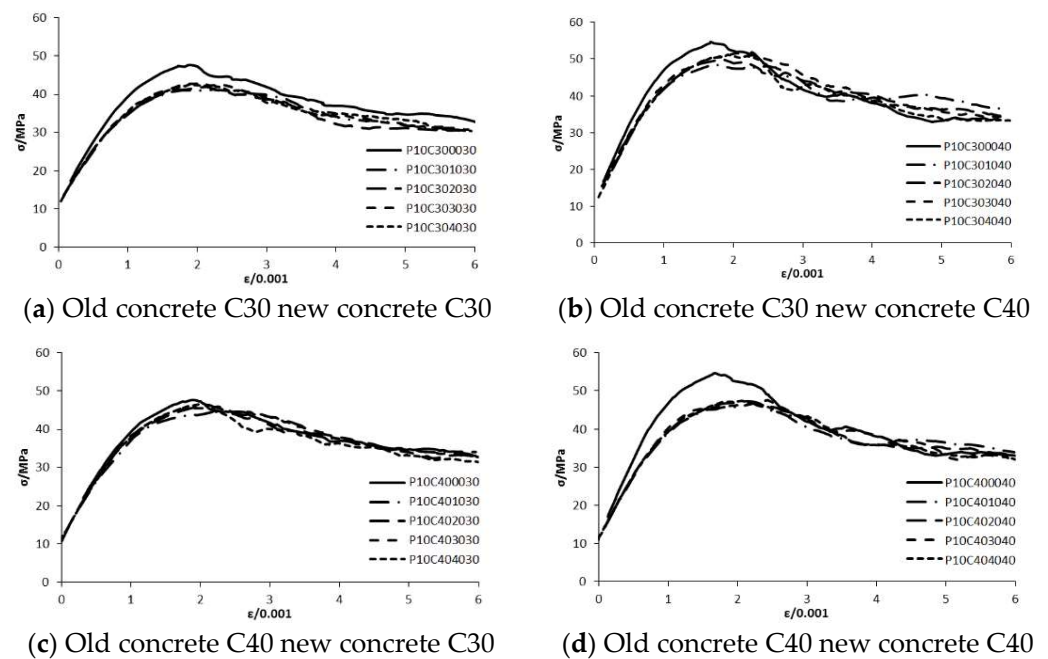

(**a**) Old concrete C30 new concrete C30

(**b**) Old concrete C30 new concrete C40

(**c**) Old concrete C40 new concrete C30

(**d**) Old concrete C40 new concrete C40

Figure 11. The stress–strain curve at 10 MPa confining pressure.

Figure 12 is the change curve of Poisson's ratio under 10 MPa confining pressure. It can be seen from the figure that the Poisson's ratio of different concretes had little difference before reaching the peak strain. After cracking, the Poisson's ratios of recycled concrete series with C40 strength new concrete and conventional concrete were quite different, while the difference from the series with 30 new concrete strength was relatively small.

The overall pressure applied to an elastomer is the volumetric stress, Θ, which can be calculated using the following equation:

$$\Theta = \sigma_x + \sigma_y + \sigma_z \tag{4}$$

The amount of change per unit volume of an elastomer is called the volumetric strain, v, which can be calculated using the following equation:

$$v = \varepsilon_x + \varepsilon_y + \varepsilon_z \tag{5}$$

Figure 13 shows the relationship curve between the volumetric stress and axial strain of the cube model when 10 MPa confining pressure is applied. In Figure 13, the ε of the x-axis is the strain in the compressive direction. It can be seen from the figure that the volume change of the series with C30 new concrete strength was greater than that of recycled aggregate, while the change of series with the C30 new concrete strength was smaller.
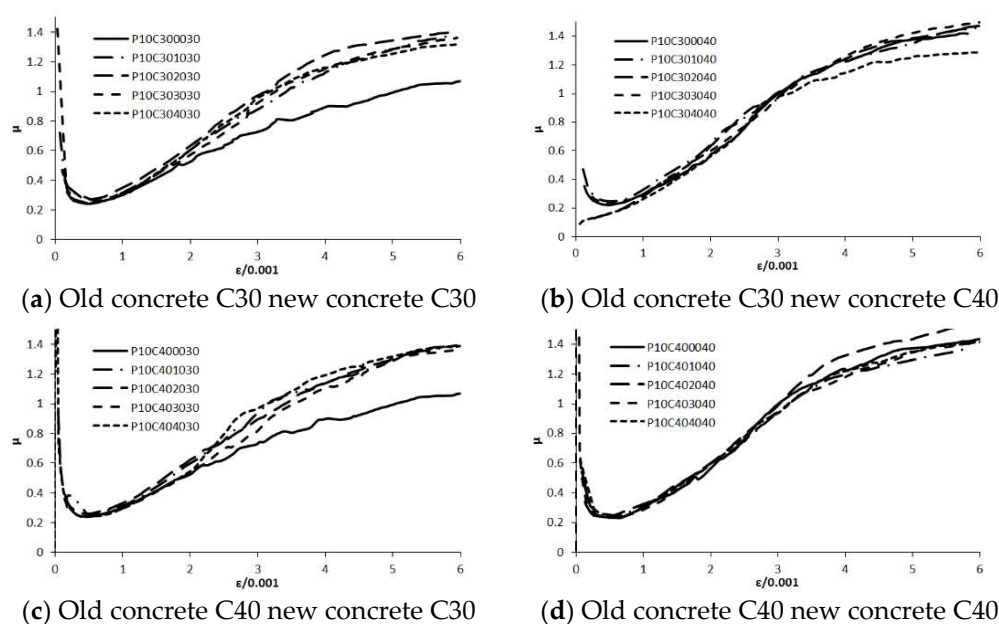
(**a**) Old concrete C30 new concrete C30

(**b**) Old concrete C30 new concrete C40

(**c**) Old concrete C40 new concrete C30

(**d**) Old concrete C40 new concrete C40

Figure 12. The relationship between Poisson's ratio and axial strain at 10 MPa confining pressure.

(**a**) Old concrete C30 new concrete C30

(**b**) Old concrete C30 new concrete C40

(**c**) Old concrete C40 new concrete C30

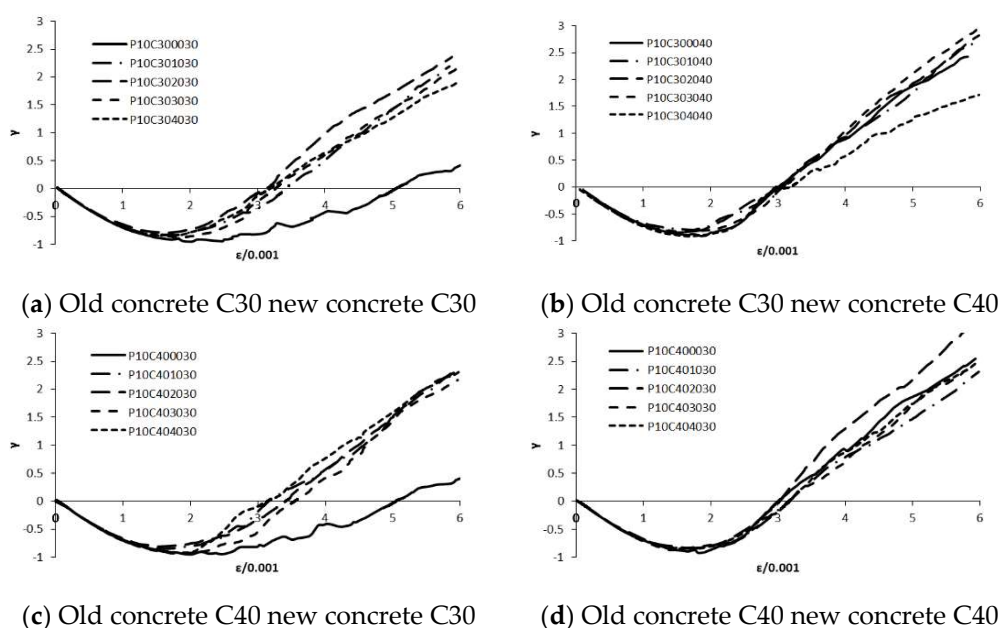(**d**) Old concrete C40 new concrete C40

Figure 13. Relationship between volume strain and axial strain at 10 MPa confining pressure.

4.3. Stress–Strain Curve under 10 MPa Confining Pressure

Two confining pressures, 10 MPa (33% of fc) and 20 MPa (67% of fc) were chosen for comparison. The compressive strength of the cube was simulated under two lateral pressures of 10 and 20 MPa, and the compressive strength under no lateral pressure is shown in Table 4. In the table, the two numbers following the letter P show the magnitude of the lateral pressure in MPa. As seen in Table 4, as lateral pressure rose, the strength of concrete with varying inclusion ratios and new and old concrete combinations increased. However, as compared to normal concrete, recycled concrete had a higher rate of improvement. When both new and recycled concrete were C30, conventional concrete gained twice the strength of unconstrained concrete and recycled concrete gained 1.2 to 1.3 times the strength of unconstrained concrete. The strength of recycled concrete was increased by

1.1 times when the old concrete was C40, and the new concrete was C30. When the old concrete was C30, and fresh concrete was C40, conventional concrete gained 0.8 times its strength, but recycled concrete gained 0.9 to 1.1 times its strength. When both the new and old concrete were C40, the strength of the recycled concrete was multiplied by 1.0 to 1.1. When the strength of new and recycled concrete was comparable, the strength gain caused by lateral pressure was more noticeable.

Figure 14 is the stress–strain curve of recycled concrete under different confining pressures. The figure lists conventional concrete with a strength of 30 MPa and recycled concrete with different incorporation ratios. Because the application field of the concrete with large-size recycled aggregate is large-volume concrete projects, some of the concrete in these projects will be subject to greater lateral pressure. Thus, the lateral pressure was taken as 0, 10, and a relatively high 20 MPa, respectively, for comparison. It can be seen from the figure that the change trend of the stress–strain curve was similar.
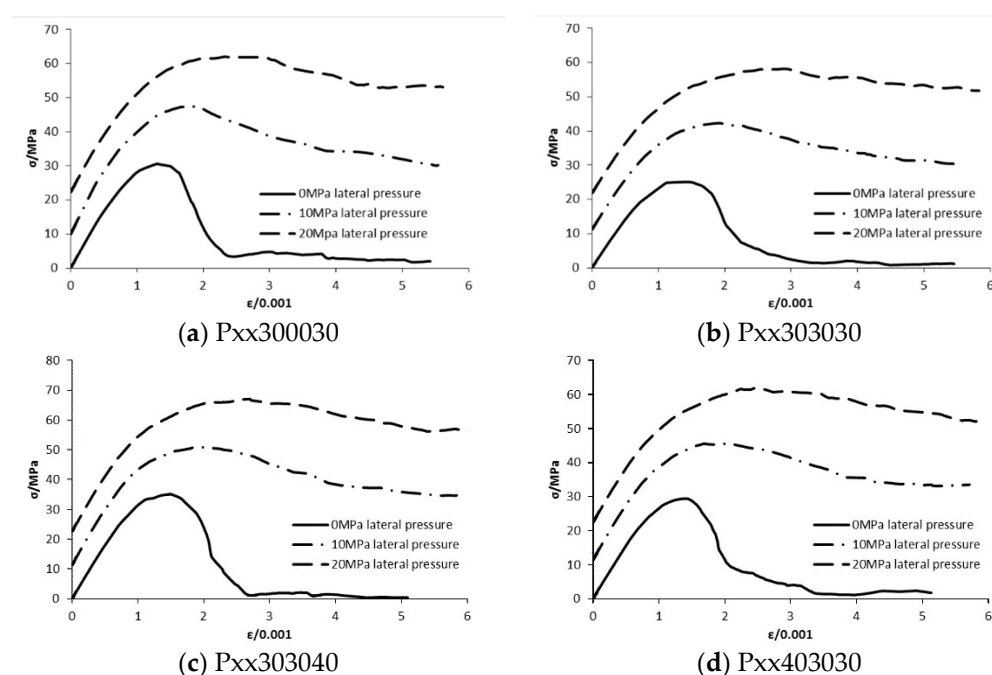

(**a**) Pxx300030   (**b**) Pxx303030

(**c**) Pxx303040   (**d**) Pxx403030

Figure 14. Stress–strain curves of different confining pressures.

The curves mentioned above were fitted using Guo's equation, with the results displayed in Table 5. It can be seen from the chart that recycled concrete has a lower rising section coefficient than conventional concrete, indicating that recycled concrete is stiffer. As confining pressure increases, both conventional and recycled concrete's coefficient values for the rising section increased. When the confining pressure was increased to 40 MPa, the coefficient of the rising section of conventional concrete approached 2.3, and the coefficient of the rising section of recycled concrete also approached this value, indicating that increasing the confining pressure effectively improves the mechanical properties of recycled concrete. Under various confining pressures, the coefficient of the descending section varied significantly. The general trend indicates that the coefficient of the descending section of recycled concrete was more significant than that of conventional concrete and that when confining pressure increased, the coefficient of the descending section increased as well. Xiao et al. [2] adjusted Guo's equation to produce the equations for rising and falling section coefficients. Under a 30% recycled aggregate incorporation ratio, the revised equation indicates that the rising section coefficient and falling section coefficient are 1.48 and 2.75, respectively. Under a 30% recycled aggregate incorporation ratio, the values obtained from simulation were 1.32 and 3.36, respectively, suitable for concrete containing a recycled aggregate of conventional size. When compared to the data in Table 5, it is clear

that when the strength of the old concrete is low and the new concrete is strong, the effect of confining pressures is more visible. This is because there are several weak points, such as the ITZ, in concrete made with large-size recycled aggregate, which is particularly porous; consequently, increasing the confining pressure significantly enhances its performance.

Table 4. Compressive strength under different confining pressures.

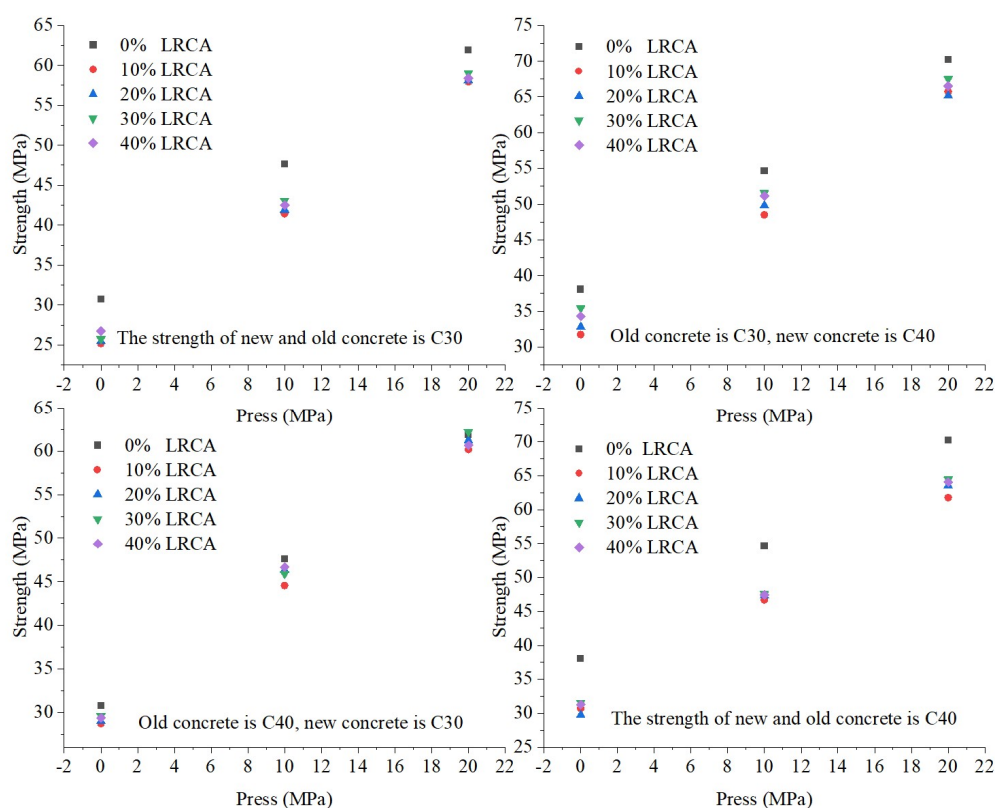| Number	Incorporation Ratio	Confining Pressure/MPa	Old Concrete Strength/MPa	New Concrete Strength/MPa	Recycled Concrete Strength/MPa
P00300030	0.00	0.00	30.00	30.00	30.73
P00300040	0.00	0.00	30.00	40.00	38.07
P00400030	0.00	0.00	40.00	30.00	30.73
P00400040	0.00	0.00	40.00	40.00	38.07
P10300030	0.00	10.00	30.00	30.00	47.66
P10300040	0.00	10.00	30.00	40.00	54.63
P10400030	0.00	10.00	40.00	30.00	47.66
P10400040	0.00	10.00	40.00	40.00	54.63
P20300030	0.00	20.00	30.00	30.00	61.90
P20300040	0.00	20.00	30.00	40.00	70.23
P20400030	0.00	20.00	40.00	30.00	61.90
P20400040	0.00	20.00	40.00	40.00	70.23
P00301030	0.10	0.00	30.00	30.00	25.17
P00301040	0.10	0.00	30.00	40.00	31.75
P00401030	0.10	0.00	40.00	30.00	28.70
P00401040	0.10	0.00	40.00	40.00	30.72
P10301030	0.10	10.00	30.00	30.00	41.42
P10301040	0.10	10.00	30.00	40.00	48.47
P10401030	0.10	10.00	40.00	30.00	44.57
P10401040	0.10	10.00	40.00	40.00	46.69
P20301030	0.10	20.00	30.00	30.00	57.95
P20301040	0.10	20.00	30.00	40.00	65.76
P20401030	0.10	20.00	40.00	30.00	60.20
P20401040	0.10	20.00	40.00	40.00	61.74
P00302030	0.20	0.00	30.00	30.00	25.43
P00302040	0.20	0.00	30.00	40.00	32.82
P00402030	0.20	0.00	40.00	30.00	28.97
P00402040	0.20	0.00	40.00	40.00	29.72
P10302030	0.20	10.00	30.00	30.00	41.92
P10302040	0.20	10.00	30.00	40.00	49.81
P10402030	0.20	10.00	40.00	30.00	46.34
P10402040	0.20	10.00	40.00	40.00	47.33
P20302030	0.20	20.00	30.00	30.00	58.12
P20302040	0.20	20.00	30.00	40.00	65.18
P20402030	0.20	20.00	40.00	30.00	61.24
P20402040	0.20	20.00	40.00	40.00	63.52
P00303030	0.30	0.00	30.00	30.00	25.73
P00303040	0.30	0.00	30.00	40.00	35.42
P00403030	0.30	0.00	40.00	30.00	29.57
P00403040	0.30	0.00	40.00	40.00	31.54
P10303030	0.30	10.00	30.00	30.00	43.08
P10303040	0.30	10.00	30.00	40.00	51.56
P10403030	0.30	10.00	40.00	30.00	45.89
P10403040	0.30	10.00	40.00	40.00	47.55
P20303030	0.30	20.00	30.00	30.00	59.04
P20303040	0.30	20.00	30.00	40.00	67.52
P20403030	0.30	20.00	40.00	30.00	62.23
P20403040	0.30	20.00	40.00	40.00	64.44
P00304030	0.40	0.00	30.00	30.00	26.72
P00304040	0.40	0.00	30.00	40.00	34.29
P00404030	0.40	0.00	40.00	30.00	29.34
P00404040	0.40	0.00	40.00	40.00	31.27
P10304030	0.40	10.00	30.00	30.00	42.50
P10304040	0.40	10.00	30.00	40.00	51.16
P10404030	0.40	10.00	40.00	30.00	46.69
P10404040	0.40	10.00	40.00	40.00	47.41
P20304030	0.40	20.00	30.00	30.00	58.42
P20304040	0.40	20.00	30.00	40.00	66.51
P20404030	0.40	20.00	40.00	30.00	60.69
P20404040	0.40	20.00	40.00	40.00	64.03

Table 5. Fitting coefficient of stress–strain curve for different confining pressures.

Number	Confining Pressure/MPa	Rising Section Coefficient	Falling Section Coefficient	R_a^2	R_f^2
P00300030	0	1.45E+00	6.65E+00	1.00E+00	9.38E−01
P10300030	10	2.11E+00	1.66E+00	1.00E+00	9.96E−01
P20300030	20	2.32E+00	4.54E−01	1.00E+00	8.61E−01
P00303030	0	2.01E+00	1.43E+01	9.95E−01	9.51E−01
P10303030	10	2.08E+00	5.65E−01	1.00E+00	9.46E−01
P20303030	20	2.47E+00	3.85E−01	9.99E−01	8.08E−01
P00303040	0	1.74E+00	4.60E+01	9.98E−01	6.06E−01
P10303040	10	2.07E+00	5.56E−01	9.99E−01	9.57E−01
P20303040	20	2.71E+00	5.32E−01	9.99E−01	9.30E−01
P00403030	0	1.82E+00	1.25E+01	9.99E−01	9.78E−01
P10403030	10	2.37E+00	7.08E−01	9.98E−01	8.53E−01
P20403030	20	2.32E+00	4.66E−01	9.98E−01	9.73E−01

Note: R_a^2 is the coefficient of determination of the rising section coefficient, R_f^2 is the coefficient of determination of the rising section coefficient.

4.4. Strength under Different Confining Pressures

The radar map in Figure 15 illustrates the compressive strength of recycled concrete at various new concrete strengths, old concrete strengths, recycled coarse aggregate incorporation ratios, and confining pressures. As illustrated in Figure 14, the incorporation ratio had a negligible effect on compressive strength, and the figure depicts five symmetrical zones.

Figure 15. Strength changes of recycled concrete with different confining pressures.

As illustrated in Figure 15, the strongest location appears to be where the old concrete was C30, and the new concrete was C40, while another point with greater strength appears to be where the recycled aggregate was C40 and the new concrete was C40. In comparison to recycled aggregate, fresh concrete had a bigger effect on the cube's compressive strength.

The two weakest spots were those where the new concrete was C30, and the model with the weakest new and old concrete had the weakest strength. Simultaneously, as the confining pressure increased, the strength of the model with the old concrete strength of C30 and the new concrete strength of C40 increased more rapidly. When the confining pressure was set to 20 MPa, the strength differential between fresh concrete and recycled aggregate decreased.

Pearson correlation was utilized to determine the relationship between the strength of recycled concrete and the integration of large-size recycled aggregate, confining pressure, and strength of old and new concrete. There were a total of 60 samples. Table 6 summarizes the test results. As shown in the table, the following elements influence the strength of recycled concrete: confining pressure, new concrete strength, incorporation ratio of large-size recycled material, and old concrete strength. The Pearson correlation coefficients were 0.96, 0.197, −0.07, and 0.006, respectively. A negative correlation coefficient shows a negative correlation.

Table 6. Correlation between factors and strength.

	Incorporation Ratio	Confining Pressure/MPa	Old Concrete Strength/MPa	New Concrete Strength/MPa
Pearson correlation	−0.07	0.96	0.006	0.197
Significance (bilateral)	0.58	0.00	0.966	0.132
N	60	60	60	60

The link between the strength of old concrete, the strength of new concrete, the incorporation ratio of large-size recycled aggregate, and the strength of recycled concrete was analyzed using partial correlation analysis with confining pressure as the control variable. Table 7 summarizes the test results. As can be observed from the table, once the confining pressure on the specimen was removed, the factor that had the largest influence on the specimen's strength was the strength of the new concrete, followed by the recycled aggregate incorporation ratio. The Pearson correlation coefficients were 0.743, −0.24, and −0.021, respectively.

Table 7. Correlation between factors and strength after removing the confining pressure.

Control Variable		Incorporation Ratio	Old Concrete Strength/MPa	New Concrete Strength/MPa
Confining pressure	Correlation	−0.24	0.021	0.743
Significance (bilateral)	Significance (bilateral)	0.06	0.873	0.000
N	df	57	57	57

The measured strength of the recycled concrete was divided into four categories based on the difference in strength between new and old concrete, and a box diagram was created as seen in Figure 16. As observed in the figure, the LP30xx30 series had the lowest overall strength, followed by the LP40xx30 series, the LP40xx40 series, and finally the LP40xx40 series. The LP40xx30 series had the smallest difference in strength, whereas the LP40xx40 series had the biggest variation in strength. The the LP40xx40 series' lesser strength than the LP30xx30 series is attributed to the data's imprecision. As seen in the figure, the peak strength of LP40xx40 was significantly more than the upper quartile strength, while the median strength was between the top and lower quartiles. As a result, when the strength of the recycled concrete is great, the stress concentration should be more apparent. The consequent localized stress concentration makes it easier to shatter the ITZ between the new and old mortar. Due to the dispersion of stress states under different compound stresses, recycled concrete's strength also exhibits increased dispersion.
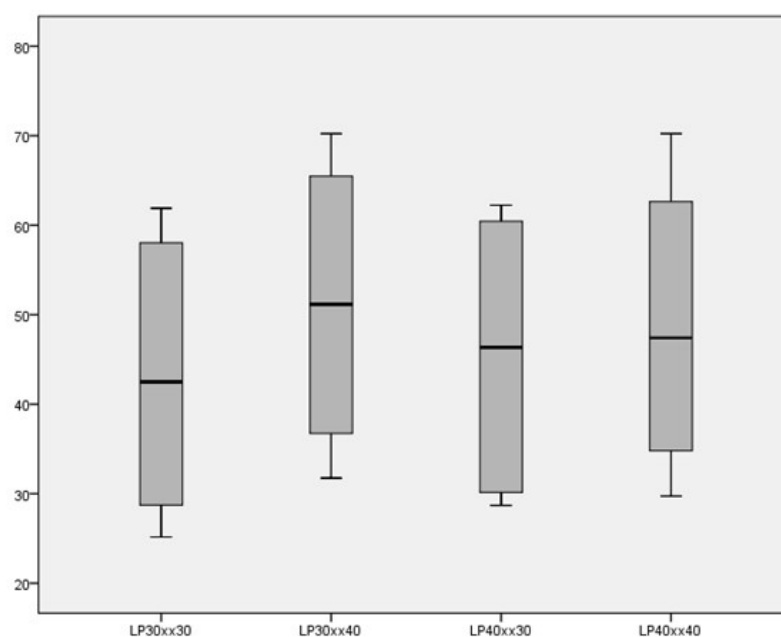
Figure 16. Strength distribution of new concrete and old concrete under different combinations.

5. Conclusions

Concerning large-size recycled aggregate concrete, where the recycled aggregate size is significantly larger than the original natural aggregate size, this article establishes a random aggregate model for concrete containing large-size recycled coarse aggregate using two-times aggregate generations. Varying confining pressures allow for establishing different recycled aggregate incorporation ratios in concrete using large-size recycled aggregate. The concept of strength was analyzed. Analyses revealed the following conclusions:

(1) In this research, the biaxial mechanical characteristics of concrete with large-size recycled aggregate were analyzed using a two-stage random aggregate creation and distribution approach. This model can more accurately describe the effect of the complex composition of large-size recycled aggregates on the cracking and strength variations of recycled concrete under confining pressure.

(2) When restricting pressure was applied, the strength of concrete containing large-sized recycled aggregate was not significantly diminished compared to tha of conventional concrete. When both new and old concrete had high strength, the recycled concrete's strength diminished proportionately more. When new concrete had a lesser strength than the existing concrete, the strength fell less. Under a confining pressure of 10 MPa, the strength of recycled concrete deteriorated the most, falling 15% below that of unrecycled concrete. The strength of recycled concrete was only 0.6 percent less than that of unrecycled concrete.

(3) When restricting pressure was applied, the fracture morphology of recycled concrete was significantly altered following the addition of large-size recycled aggregate. Cracks in standard concrete were square and had an angle of around 45 degrees with a horizontal direction. As the proportion of large recycled aggregates rose, the model's crack count climbed. The model's cracks eventually transitioned from the ITZ to a diagonal crack that penetrated two opposing corners.

(4) When confining pressure was applied, the addition of large-size recycled aggregate had a bigger effect on the rising region of the stress–strain curve but a relatively lower effect on the falling section. When the age of the concrete was greater than the age of the new concrete, adding large-size recycled aggregate did not affect the stress–strain curve. When the old and new concrete strengths were equal, the stress–strain curve's rising portion had a higher reduction.

(5)   When the stress–strain curve was fitted using Guo's equation and the coefficients of Xiao's equation were compared, it was observed that as confining pressure is increased, the rising section coefficient of the stress–strain curve of large-size recycled aggregate concrete gradually increased. When the strength of the old concrete was low and the new concrete was strong, the influence of confining forces was more visible.

(6)   When confining pressure was applied, the following elements affected the strength of recycled concrete: confining pressure, new concrete strength, incorporation ratio of recycled coarse aggregate, and strength of old concrete. The Pearson correlation coefficients calculated using this study's simulation results were 0.96, 0.197, −0.07, and 0.006, respectively.

Author Contributions: Conceptualization, J.X.; methodology, T.L.; writing—original draft preparation, T.L.; writing—review and editing, T.L. and J.X.; supervision, J.X.; funding acquisition, T.L. and J.X. All authors have read and agreed to the published version of the manuscript.

Institutional Review Board Statement: Not applicable.

Informed Consent Statement: Not applicable.

Data Availability Statement: Data is contained within the article or supplementary material.

Conflicts of Interest: The authors declare no conflict of interest.

Notation

E_c	Interparticle contact modulus
k_n/k_s	Ratio of particle normal and tangential stiffness
$\overline{\mu}$	Particle friction coefficient
$\overline{\lambda}$	Parallel bonding radius multiplier
$\overline{E}_c$	Parallel bonding modulus
$\overline{k}_n/\overline{k}_s$	Ratio of parallel bonding normal and tangential stiffness
$\overline{\sigma}_c(mean)$	Average normal strength of parallel bonding
$\overline{\sigma}_c(std.dev)$	Standard deviation of normal strength of parallel bonding
$\overline{\tau}_c(mean)$	Average tangential strength of parallel bonding
$\overline{\tau}_c(std.dev)$	Standard deviation of tangential strength of parallel bonding

References

1.   Levy, S.M.; Helene, P. Durability of recycled aggregates concrete: A safe way to sustainable development. *Cem. Concr. Res.* **2004**, *34*, 1975–1980. [CrossRef]
2.   Xiao, J.; Li, J.; Zhang, C. Mechanical properties of recycled aggregate concrete under uniaxial loading. *Cem. Concr. Res.* **2005**, *35*, 1187–1194. [CrossRef]
3.   Etxeberria, M.; Vazquez, E.; Mari, A.; Barra, M. Influence of amount of recycled coarse aggregates and production process on properties of recycled aggregate concrete. *Cem. Concr. Res.* **2007**, *37*, 735–742. [CrossRef]
4.   Domingo-Cabo, A.; Lázaro, C.; López-Gayarre, F.; Serrano-López, M.A.; Serna, P.; Castaño-Tabares, J.O. Creep and shrinkage of recycled aggregate concrete. *Consrt. Build. Mater.* **2009**, *23*, 2545–2553. [CrossRef]
5.   Poon, C.S.; Shui, Z.H.; Lam, L. Effect of microstructure of ITZ on compressive strength of concrete prepared with recycled aggregates. *Consrt. Build. Mater.* **2004**, *18*, 461–468. [CrossRef]
6.   Casuccio, M.; Torrijos, M.C.; Giaccio, G.; Zerbino, R. Failure mechanism of recycled aggregate concrete. *Consrt. Build. Mater.* **2008**, *22*, 1500–1506. [CrossRef]
7.   Limbachiya, M.C.; Leelawat, T.; Dhir, R.K. Use of recycled concrete aggregate in high-strength concrete. *Mater. Struct.* **2000**, *33*, 574. [CrossRef]
8.   Kou, S.C.; Poon, C.S. Properties of self-compacting concrete prepared with coarse and fine recycled concrete aggregates. *Cem. Concr. Comp.* **2009**, *31*, 622–627. [CrossRef]
9.   Li, T.; Xiao, J.; Zhu, C.; Zhong, Z. Experimental study on mechanical behaviors of concrete with large-size recycled coarse aggregate, Consrt. *Build. Mater.* **2016**, *120*, 321–328. [CrossRef]

10.   Pulatsu, B.; Bretas, E.M.; Lourenço, P.B. Discrete element modeling of masonry structures: Validation and application. *Earthq. Struct.* **2016**, *11*, 563–582. [CrossRef]

11.   Sarhosis, V.; Lemos, J.V. Detailed micro-modelling of masonry using the discrete element method. *Comput. Struct.* **2018**, *206*, 66–81. [CrossRef]

12.   Sarhosis, V.; Forgcas, T.; Lemos, J.V. A discrete approach for modelling backfill material in masonry arch bridges. *Comput. Struct.* **2019**, *224*, 106–118. [CrossRef]

13.   Ferretti, E.; DECM. A Discrete Element for Multiscale Modeling of Composite Materials Using the Cell Method. *Materials* **2020**, *13*, 880. [CrossRef]

14.   He, Z.J.; Ding, M.J.; Zhang, X.J. The Biaxial Compressive Mechanical Properties and Strength Criterion of Recycled Aggregate Concrete under Different Dynamic Strain Rates. *Iran. J. Sci. Technol.* **2020**, *45*, 1–22. [CrossRef]

15.   Ying, L.; Peng, Y.; Kamel, M. 3-D base force element method on meso-damage analysis for recycled concrete. *Struct. Concr.* **2021**. [CrossRef]

16.   Yu, Y.; Zheng, Y.; Zhao, X.Y. Mesoscale modeling of recycled aggregate concrete under uniaxial compression and tension using discrete element method. *Constr. Build. Mater.* **2020**, *268*, 121116. [CrossRef]

17.   Peng, Y.J.; Wu, Z.H.; Ying, L.P.; Yang, D.S. Five-phase sphere equivalent model of recycled concrete and numerical simulation based on the base force element method. *Eng. Comput.* **2020**. [CrossRef]

18.   Tan, X.; Hu, Z.; Li, W. Micromechanical Numerical Modelling on Compressive Failure of Recycled Concrete using Discrete Element Method (DEM). *Materials* **2020**, *13*, 4329. [CrossRef] [PubMed]

19.   Li, T.; Xiao, J.Z. Simulation on Compressive Property of Concrete with Large-Size Recycled Coarse Aggregate. *ACI Mater. J.* **2016**, *117*, 159–168.

20.   Ravindrarajah, R.; Tam, C.T. Properties of concrete made with crushed concrete as coarse aggregate. *Mag. Concr. Res.* **1985**, *37*, 29–38. [CrossRef]

21.   Liu, Y.; Cai, M.F.; Yang, Z.J. Study on deterioration law of rock strength parameters based on PFC simulation method. In *Rock Mechanics: Achievements and Ambitions-Proceedings of the 2nd ISRM International Young Scholars' Symposium on Rock Mechanics*; Cai, M.F., Ed.; CRC Press: Beijing, China, 2012; pp. 151–154.

22.   Funk, J.E.; Dinger, D.R. Particle packing part I: Fundamentals of particle packing monodisperse spheres. *Interceram* **1992**, *41*, 10–14.

23.   Dinger, D.R.; Funk, J.E. Particle packing, part II: Review of packing polydisperse particle system. *Interceram* **1992**, *41*, 95–97.

24.   Dinger, D.R.; Funk, J.E. Particle packing, part III: Discrete versus continuous particle sizes. *Interceram* **1992**, *41*, 332–334.

25.   Dinger, D.R.; Funk, J.E. Particle packing, part IV: Computer of modelling particle packing phenomen. *Interceram* **1993**, *42*, 150–153.

26.   Dinger, D.R.; Funk, J.E. Particle packing, part V: Computational methods applied to experimental distributions. *Interceram* **1994**, *43*, 87–89.

27.   China Academy of Building Research. *Standard for Method of Concrete Structure (GB/T 50152–2012)*; Ministry of housing and urban-rural development of People's Republic of China: Beijing, China, 2012.